Hindawi
Mobile Information Systems
Volume 2023, Article ID 4449959, 10 pages
https://doi.org/10.1155/2023/4449959

Research Article

Convoluted Meander Line-Inspired Metallic Surface Filter for Bluetooth and WLAN Bands

Ashish Bagwari,[1,2] **Payal Jindal**,[3] **Ajay Yadav**,[4] **Rahul Tiwari**,[1,2] **Sudhir Kumar Sharma**,[5] **and J. Logeshwaran**[6]

[1]*Department of Electronics and Communication Engineering, Uttarakhand Technical University, Dehradun, India*
[2]*Department of Electronics and Communication Engineering, WIT, Uttarakhand Technical University, Dehradun, India*
[3]*Department of ECE, Poornima College of Engineering, Jaipur, Rajasthan, India*
[4]*Department of ECE, Jaipur Engineering College and Research Centre, Jaipur, Rajasthan, India*
[5]*Department of ECE, Jaipur National University, Jaipur, Rajasthan, India*
[6]*Department of ECE, Sri Eshwar College of Engineering, Coimbatore, Tamil Nadu, India*

Correspondence should be addressed to Ashish Bagwari; ashishbagwari@gmail.com

Received 27 May 2022; Revised 10 May 2023; Accepted 24 May 2023; Published 6 June 2023

Academic Editor: Zahid Mehmood

A convoluted meander line integrated cross dipole metallic structure with a dual-bandstop feature is presented in this manuscript. The investigated frequency-selective surface (FSS) exhibits the bandstopping characteristics for the Bluetooth (2.4 GHz) and WLAN (5.5 GHz) applications with a miniaturized unit cell size of $9.7 \times 9.7\ mm^2$. The proposed design has a polarization insensitivity feature for the TE and TM polarized waves' incidents at 0°–60° with an interval of 15° angle. The equivalent circuit model of the presented FSS unit cell is also discussed and their limped element values are presented. The FSS design has a compact size which makes it favorable for low-profile band-filtering systems and multipath EM wave's insensitivity. The suggested FSS configuration has good correspondence with modelled and measured results.

1. Introduction

In the present wireless communication scenario for short-range such as Bluetooth, WLAN and WiMAX are very popular. These narrowband applications significantly contributed to electromagnetic interference in short-range communication systems that operate on very low power. Nowadays, short-range RADARs are also used for proximity detection and data transmission applications using free-space communication mediums. However, to utilize the advantages of UWB or short-range RADAR applications, it is essential to make EMI-free environment by placing FSS as shielding for the devices. These devices are designed in a compact size to minimize the complexity and follow the IEEE standard 802.11 [1]. Our daily life has become significantly easier and more comfortable due to wireless devices. However, electromagnetic radiation from these wireless devices harms the human body and cannot be discounted. The electromagnetic radiation infiltrates the human body and may be a source of cancer and many medical sicknesses previously highlighted by authorities and researchers [2, 3].

An FSS may be defined as an array of resonating small unit cells that may pass the specific frequency band, whereas behaving like a bandstop filter for other frequency bands. An FSS also accommodates all the scattering characteristics such as reflection, absorption, and transmission, which are a function of frequency. The electromagnetic wave filtering can be accomplished by the resonator shape, periodic metallic design, or stacking of dielectric faces [1].

Recently, different kinds of FSS structures have been introduced for filtering applications. For example, circular shape, rectangular resonating structure, dipoles, cross dipoles, tripole, Jerusalem cross, and three- or four-leg FSS

dipoles [1, 4, 5]. The FSS is designed to stop or pass the specific frequency band according to the requirement of the applications [1–6]. FSS is also known as a spatial filter which is generally used to select the polarization and filtering of desired frequency; however, FSS includes a sufficient number of periodic resonating structures in practice. Several FSS designs with single or multiband characteristics have been investigated in [6–12]. To mitigate the interference between WLAN and other adjacent wireless applications for wireless security, a comprehensive investigation has been explored in [6, 8–12].

Due to electromagnetic (EM) waves' multipath propagation characteristics, it is not always possible to implement an FSS structure perpendicular to the incident EM wave. This practical limitation of FSS causes the unstable and perturbed response which is essential to avoid in bandstop FSS applications under oblique incidents of EM waves. The polarization insensitivity of the FSS is highly desirable for practical applications, such as absorbers, reflectors, polarization converters, AMC, and EM shielding beam shaping. This highly demanded characteristic of FSS is optimized and presented through the state of art by several researchers in [13–22, 22].

A triple-band notched polarization-independent compact FSS is a filter designed to attenuate specific frequency bands while allowing other frequency bands to pass through. This type of filter is often used in ultra-wideband (UWB) applications as its broadband capabilities allow for more excellent signal coverage and transmission. The filter combines metallic and dielectric materials carefully arranged in a particular pattern. This pattern allows the filter to reduce the amplitude of specific frequency bands and operate independently for both linear- and circular-polarized waves. This type of filter offers advantages such as a reduced size compared to traditional filters, improved performance for UWB applications, and higher power handling capabilities. The design of such a filter must consider several considerations, such as the size, the number of elements, the material used, the periodicity, the polarization, and the temperature stability, among other things. Additionally, the filter must be designed to account for reflections, scattering, and radiation. [23].

The design and analysis of a single-sided modified square loop UWB frequency-selective surface (FSS) is an important research area in electromagnetic engineering. It involves the design of frequency-selective surfaces (FSSs) with high selectivity, low insertion loss, and good impedance matching. FSSs are thin metallic surfaces structured to selectively reflect and absorb electromagnetic signals with specific frequencies while allowing other signals to pass through. The single-sided modified square loop FSS is a type of FSS comprising two square loop resonators connected with a dielectric slab. It offers a good impedance match, a wide frequency band, and a good response. The FSS is designed using computer-aided software such as CST Microwave Studio, and parameters such as the gap between elements, the size of the elements, and the dielectric material can be optimized. The performance of FSSs is usually measured in terms of insertion loss, return loss, and isolation. The design and analysis of these FSSs allow them to be used successfully in applications such as wireless communication systems, ultra-wideband systems, and automotive radar systems [24].

A frequency-selective surface (FSS) is an advanced metallic structure that can reflect or pass electromagnetic energy of a specific frequency. They are commonly used for beam steering, antenna isolation, antenna gain enhancement, and antenna noise reduction. The analysis and design of a bandstop FSS at the mobile WiMAX and X-band for satellite communication is a challenging task due to the specific requirements of the application. The primary goal of the design is to achieve maximum suppression of the undesired signals while still allowing the desired signal to pass. An FSS is usually designed by optimizing the surface's size, shape, and materials to achieve the desired performance. The first step is identifying the desired frequency range that must be rejected. Then, the size and shape of the surface can be determined based on the frequency range and the required characteristics, such as minimum and maximum rejection of the undesired signal. A combination of mathematical modeling, simulation, and testing will then determine the size and shape of the surface. The materials are selected based on the frequency range, and an analysis is performed of the properties of the materials to ensure that they will meet the desired performance goals. The material properties must also be tested to ensure that the surface achieves the desired performance. The results from these tests and analyses are used to refine the design and manufacturing of the surface [25].

This manuscript explores the performance investigation of an FSS design that displays the double bandstop characteristics and polarization insensitivity of incident EM wave up to 60°. The conventional cross dipole-shaped metallic strip is integrated with convoluted meander-shaped metallic structure. The novelty of this design is that the traditional cross dipole structure is further integrated with a convoluted meander-shaped metallic patch, which alters the effective inductance and capacitance of the overall design to produce the double bandstop features for Bluetooth and WLAN applications. The demonstrated FSS model has an acceptable double bandstop characteristic, and it also shows the miniaturized unit cell size for low-frequency applications such as Bluetooth at 2.4 GHz. The proposed FSS can provide complete shielding from the highly used Bluetooth/WLAN devices for both the bands 2.4 and 5.5 GHz.

2. Design and Equivalent Circuit Model of the Dual-Band FSS

The unit cell geometry of the proposed FSS is presented in Figure 1, which comprises of convoluted metallic meander shape on one side of the substrate. The meander shape is connected with the central cross-metallic pattern, and each end of the cross is connected with a nonperiodic meander design. The nonperiodic nature of the meander design provided the degree of freedom to vary the effective inductance and coupling capacitance. The proposed nonperiodic shape of the meander makes it favorable to achieve the low-frequency bandstop features. The design variables of

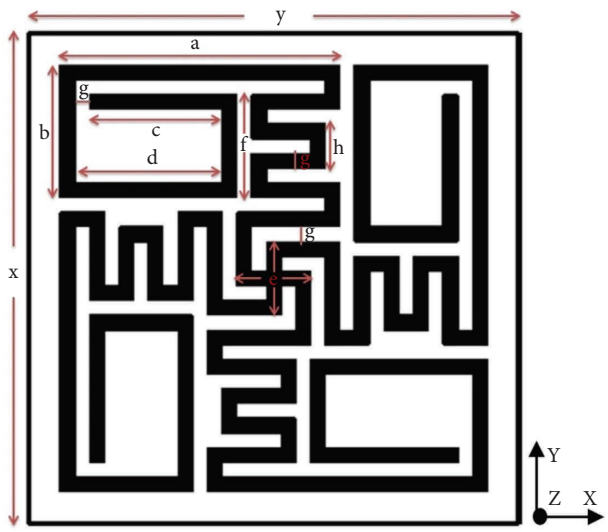

Figure 1: Simulated snapshot of proposed FSS design for Bluetooth and WLAN bands ($x = y = 9.7$ mm, $a = 5.7$ mm, $b = c = 2.7$ mm, $d = 3.0$ mm, $e = 1.5$ mm, $f = 2.1$ mm, $g = 0.3$ mm, and $h = 0.9$ mm).

the proposed FSS unit cell are mentioned in Figure 1. The presented FSS is etched on a 1.6 mm thick FR4 substrate with a dielectric constant of 4.4 and a loss factor of 0.02. The proposed FSS unit cell has a compact size of $0.0776\lambda \times 0.0776\lambda$ calculated at the lower resonant frequency of 2.4 GHz.

The equivalent lumped circuit model of the proposed FSS unit cell is exhibited in Figure 2. The effective total inductance and capacitance due to the meander-shaped metallic structure and cross pattern are presented as L and C, respectively. The effective capacitance included the capacitance due to gap between the convoluted meander lines. Under the influence of vertical polarization, the electric field is aligned in Y-direction, and it produces two parallel combinations of series LC resonators.

The equivalent circuit model produces the dual-band resonance at 2.4 GHz and 5.5 GHz, and the resonance frequency (f_0) can be calculated for each series LC resonator with the following equation:

$$f_0 = \frac{1}{(2\pi\sqrt{\mathrm{LC}})}. \tag{1}$$

The resonance frequency of the stop band can be controlled by increasing/decreasing either the inductance or capacitance or both of the FSS structures. The increase in metallic meander-shaped length increases the inductance, and small gap size between successive unit cells may increase the capacitance. Likewise, the FSS structure should be polarization-insensitive as well as produce angular stability for practical applications.

The calculated value for inductance and capacitance at 2.4 GHz resonance from the equivalent circuit model as $L_2 = 4.3$ nH and $C_2 = 1.05$ pF, and similarly at 5.5 GHz, the values are $L_1 = 2.36$ nH and $C_1 = 0.35$ pF. The corresponding filtering nature of the lumped model and simulated FSS is compared and shown in Figure 3; the simulated FSS result is in agreement with the lumped model simulated result. The characteristic or impulse transient function is determined by the response of the circuit to the function. Like the transient response, it has several types, which are determined by the type of impulse and response-voltage or current. Generally, impulse response is represented as follows. It does not have independent power sources; it is the ratio of the response of this circuit to the impact of a nonunit current or voltage jump to the height of this jump under zero initial conditions: the transient response of the circuit is numerically equal. The dimension of the transient response is equal to the ratio of the dimension of the response to the dimension of the external action, so the transient response can be resistive, conductance, or a dimensionless quantity.

The dielectric substrate acts as a transmission line with a Z_d characteristic impedance and length of 1.6 mm (thickness "t"). The characteristic impedance of the assumed transmission line can be calculated as $Z_d = (Z\_0/\sqrt{(\varepsilon\_r)})$, where Z_0 is free-space impedance and around 377 Ω, and ε_r is the relative permittivity of the substrate. The dielectric loss during the transmission from FSS is represented by "R_d," and it varies from 2 to 8 Ω for FR4 substrate. The input impedance of the transmission line model is presented as Z_{in} and can be calculated by the following equation:

$$Z_{\mathrm{in}} = \frac{1}{\left((1/(j\omega L + (1/j\omega C))) + \left(Z_d + \mathrm{j}Z_0 \tan\beta t\right)/\left(Z_d\left(Z_0 + \mathrm{j}Z_d \tan\beta t\right)\right)\right)}. \tag{2}$$

The reflection and transmission coefficients can be described as

$$\Gamma = \frac{(Z\_\mathrm{in} - Z\_0)}{(Z\_\mathrm{in} + Z\_0)}, \qquad T = 1 - \Gamma, \tag{3}$$

where ω is the angular frequency, β represents the propagation constant in the medium, and "t" is the thickness of the dielectric medium.

The thickness of dielectric medium is very little in comparison to wavelength, so $\tan\beta t$ is taken as zero in equation (2). Then, the reflection coefficient Γ can be described as

$$\Gamma = \frac{(-Z\_0)}{(Z\_0 + 2(j\omega C + 1/j\omega L))}. \tag{4}$$

Based on the equivalent circuit model, the convoluted meander-shaped dual-band FSS can be simulated in the full-wave simulator, and the proposed FSS is simulated in CST Microwave Studio.

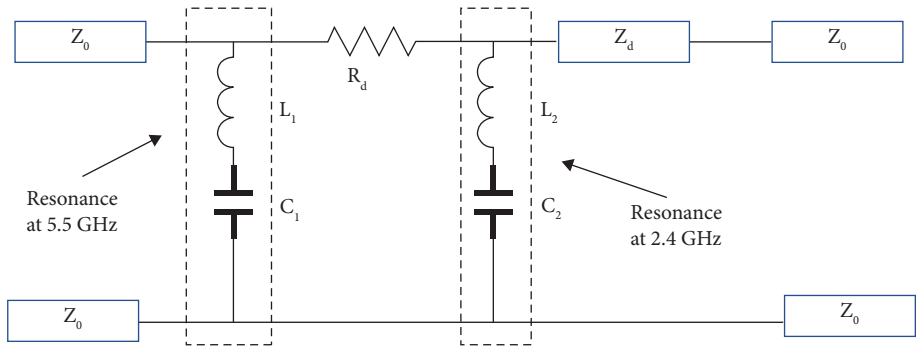

Figure 2: Equivalent circuit model of the proposed FSS unit cell.

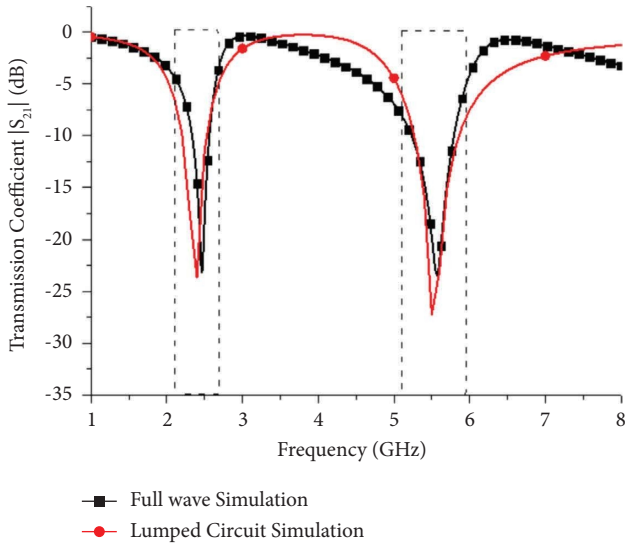

Figure 3: Transmission coefficient of the proposed FSS unit cell calculated from ECM and full-wave simulation (CST).

The equilibrium state of the pendulum is equal to the state of the circuit when the capacitor is discharged. At this time, the elastic force disappears, and there is no voltage on the capacitor in the circuit. The potential energy of elastic deformation of the spring and the energy of the electric field of the capacitor are equal to zero. The energy of the system consists of the kinetic energy of the load or the energy of the magnetic field of the current. The discharge of the capacitor continues as motion to the extreme equilibrium state. The process of recharging the capacitor is similar to the process of moving the load from the equilibrium state to the extreme state. Hence, the total energy of the system is determined as

$$E = E_P + E_K = \frac{kx^2}{2} + \frac{mv^2}{2},$$
$$W = W_P + W_K = \frac{q^2}{2C} + \frac{LI^2}{2}. \quad (5)$$

A simple system in which natural electromagnetic oscillations are possible is called an oscillating circuit consisting of a capacitor and an inductor connected to each other. The strength of the electric field in a capacitor determines how much energy changes accompany natural oscillations in the circuit, much like a mechanical oscillator like a large body on an elastic spring. The analogue of the kinetic energy of a moving body is energy in a magnetic field. In fact, the energy of the spring is proportional to the square of the displacement from the equilibrium position, and the energy of the capacitor is proportional to the square of the charge. The kinetic energy of a body is proportional to the square of its velocity, and the energy of the magnetic field in the coil is proportional to the square of the current. There is more to consider than just a formal similarity between the quantities describing oscillatory processes and circuit processes, and the extreme states are equal to the state of the circuit when the charge of the capacitor is maximum.

3. Simulated Results of Dual-Bandstop FSS

The proposed FSS unit cell is designed to stop the Bluetooth and WLAN frequencies, and its simulated snapshot is presented in Figure 1. The FSS prototype is fabricated on the FR4 dielectric material with 1.6 mm thickness, relative permittivity $\varepsilon_r = 4.4$, and dielectric loss factor of 0.02. A modified conventional cross-metallic strip integrated with a convoluted meander-shaped metallic strip is etched to produce a dual-bandstop feature for Bluetooth and WLAN applications. The overall size of the unit cell is $0.0776\lambda \times 0.0776\lambda$ and it is a single-side printed configuration of the FSS.

The transmission and reflection characteristics of the proposed FSS design are presented in Figure 4. It displays that the proposed FSS creates negligible transmission at 2.4 and 5.5 GHz. The FSS has covered the WLAN frequency spectrum ranging from 5.1 GHz to 5.8 GHz. It also presents the negligible transmission for frequency spectrum ranging from 2.3 to 2.5 GHz, which comprises the Bluetooth/WLAN band for short-range wireless applications. Proposed FSS exhibits angular consistency for transverse electric and polarized magnetic waves for angle varying from 0° to 60°.

Figure 4 shows that the proposed FSS produces satisfactory band-filtering features and its −3 dB bandwidth has a wide spectrum that accommodated the complete Bluetooth and WLAN bands. At 2.4 GHz and 5.5 GHz, it has a transmission coefficient of −23.96 dB. The reflection coefficient is very high for Bluetooth and WLAN band spectrum; it shows that the FSS design reflects these frequency bands.

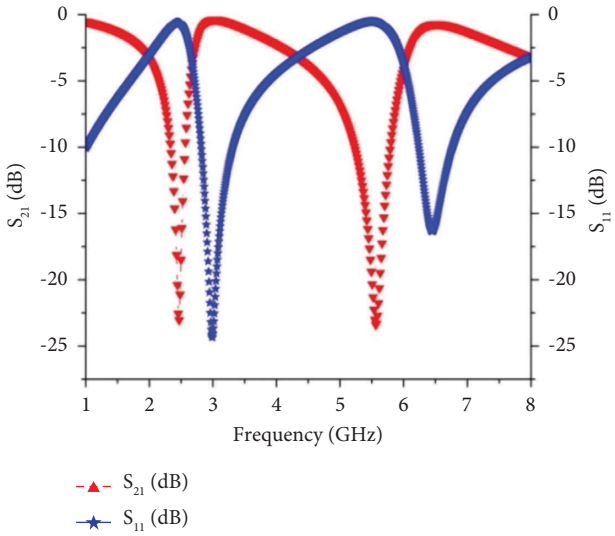

Figure 4: Reflection and transmission coefficient characteristics of proposed FSS.

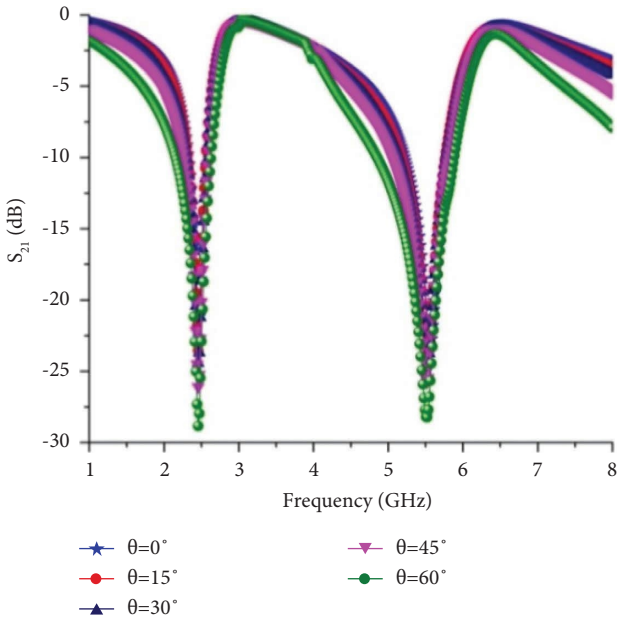

Figure 5: Transverse electric mode transmission coefficient at different angles.

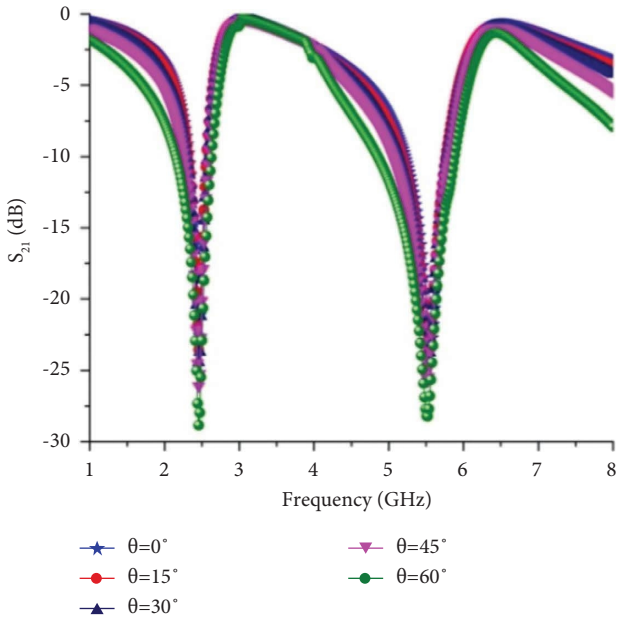

Figure 6: Transverse magnetic mode transmission coefficient at different angles.

The symmetrical design of FSS makes it polarization-insensitive and produces negligible variation with incident angles of the polarized wave. An investigation of polarization insensitivity of proposed FSS with TE polarized incident wave at different angles are exhibited in Figure 5. It shows that the transmission coefficient of investigated FSS has an insensitive behavior for TE polarized waves over a range of incident angles which varies from 0° to 60° with an angular difference of 15°.

Additionally, the suggested FSS has also tested for the transverse magnetic polarized incident wave, and the transmission coefficient results are exhibited in Figure 6. It is observed that the proposed FSS has no variation in its transmission characteristics during an incident of TM polarized wave from different directions. The results presented in Figures 5 and 6 verify that the proposed FSS design is insensitive to the incident of polarized waves from different directions.

The surface current characteristics of the proposed dual-bandstop FSS are exhibited in Figure 7. It is evidenced that for lower resonance frequency (2.4 GHz), huge surface current concentration near the outer edges and inner part of the meander line increases the effective inductance and resulted in resonance at a lower frequency. The surface current concentration only in the inner part of the meander line lowers the effective inductance and produces resonance at a higher frequency (5.5 GHz). A circuit's time characteristic is a function of time whose values are determined numerically by the circuit's response to a typical action. The response of a circuit to a given typical operation depends only on the circuit diagram and the parameters of its elements and, therefore, can act as its characteristics. Time characteristics are determined for linear circuits with no independent power sources and under zero initial conditions. Temporal characteristics depend on the type of specific general impact. If the action is given in the form of a single voltage jump and the reactance is also a voltage, the transient response is dimensionless, numerically equal to the voltage at the output of the circuit, and called the transient function or transfer coefficient. The convoluted meander line is a type of waveguide that is used to filter signals at specific frequencies. This waveguide type comprises a series of bends and turns that create an inductive-capacitive (LC) filter. The waveguide structure is designed to form a band-pass filter capable of filtering signals within specific frequencies. The design of the meander line filter is used to control the resonant frequency of the waveguide. The waveguide is

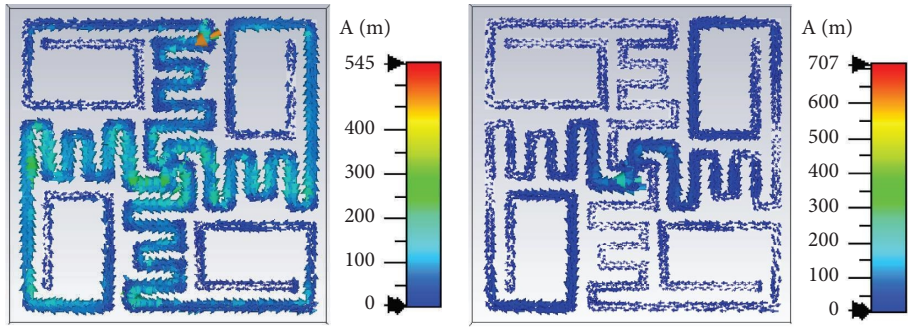

Figure 7: Surface current distribution at different frequencies. (a) 2.4 GHz. (b) 5.5 GHz.

constructed with a variable number of turns to create a variable inductance, which will determine the frequency of the filter. The capacitance of the filter is determined by the size of the waveguide and the amount of dielectric material used. The meander line filter filters out signals in the Bluetooth and WLAN bands. The filter is designed to have a loss in the Bluetooth and WLAN bands while allowing signals in other bands to pass through. It creates a band gap, which is the difference between the frequencies allowed to pass through and those blocked. The metallic surface filter is designed by creating a pattern of alternating meander lines on the surface of a metallic substrate. It creates an array of capacitors and inductors, which filter out the specific frequencies in the Bluetooth and WLAN bands. The capacitance and inductance of the filter are determined by the size and shape of the meander lines and by the amount of dielectric material used in the filter. The band gap is obtained by designing the meander lines to create a filter with a specific resonant frequency. The resonant frequency will determine the frequencies allowed to pass through the filter while blocking out other frequencies. It creates a band gap between the frequencies that are allowed to pass through and the frequencies that are blocked. The meander line filter creates a metallic surface filter for Bluetooth and WLAN bands. The filter is designed to have a loss in the Bluetooth and WLAN bands while allowing signals in other bands to pass through. It creates a band gap, which is the difference between the frequencies allowed to pass through and those blocked. The band gap is obtained by designing the meander lines to create a filter with a specific resonant frequency.

4. Measured Results and Discussions

To authenticate the working of the suggested FSS, a model has been fabricated on the FR4 substrate. The FSS fabricated model ($15 \times 10\ \text{cm}^2$) is exhibited in Figure 8, and it comprises an array of 20×20 unit cells. The fabricated prototype is utilized to verify the simulated characteristics with measured ones such as S_{11} and S_{21} of suggested FSS. The free-space measuring technique is applied to measure the transmission/reflection coefficient of the FSS; in this technique, two identical double-ridged high gain horn antennas were used during the normal incident of EM waves on proposed FSS. The free-space measurement technique (without any structure) is implemented and background signal power is recorded before the test FSS installation. After the implementation of test FSS again, signal power level is recorded, and without FSS, power level is subtracted to calculate the transmission coefficient of test FSS. The measured and computer model-based simulated results compared findings which are shown in Figure 9. A small deviation amongst the simulated and measured outcomes is detected that are due to a small error in measurement setup losses and tolerances during fabrication. The measured result closely trails the simulated one. It also validates the suggested FSS to limit the EM signal transmission in the Bluetooth and WLAN bands.

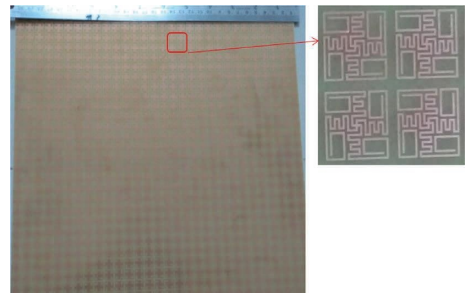

Figure 8: Fabricated model of FSS array.

A compared S_{11} (dB) result of the proposed FSS is depicted in Figure 10. The proposed FSS model displays the effective dual-band notch creation with sufficient wide bandwidth. From Figure 10, it can be seen that measured and simulated S_{11} outcomes are close in nature and it permits other bands to pass excluding the Bluetooth band and WLAN band.

Two similar horn antennas have been applied in the practical measurement and a true measurement setup is shown in Figure 11, which displays the actual measuring arrangement for the suggested FSS model. The distance between both the horns and FSS prototype is adjusted in such a way to maintain the far field with respect to the corresponding frequency of FSS.

The fabricated model has been measured for transverse electric and polarized magnetic waves under oblique incidence. The measured results also confirm that the suggested FSS has angular consistency, and its transverse electric and magnetic polarization results are presented in

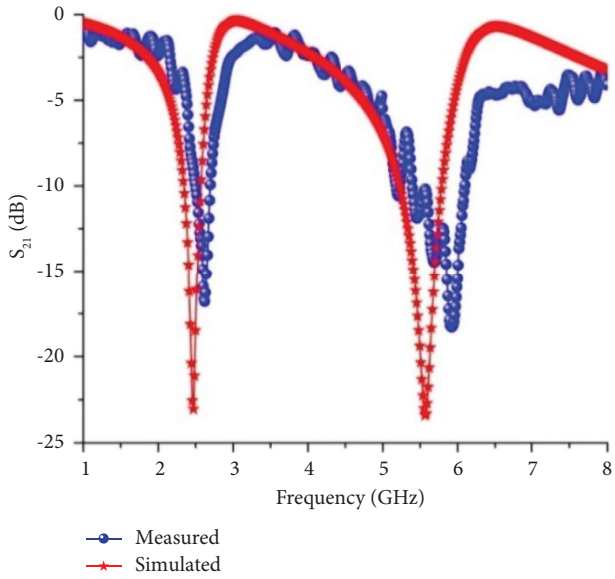

Figure 9: Measured and simulated S_{21} (dB) vs. frequency.

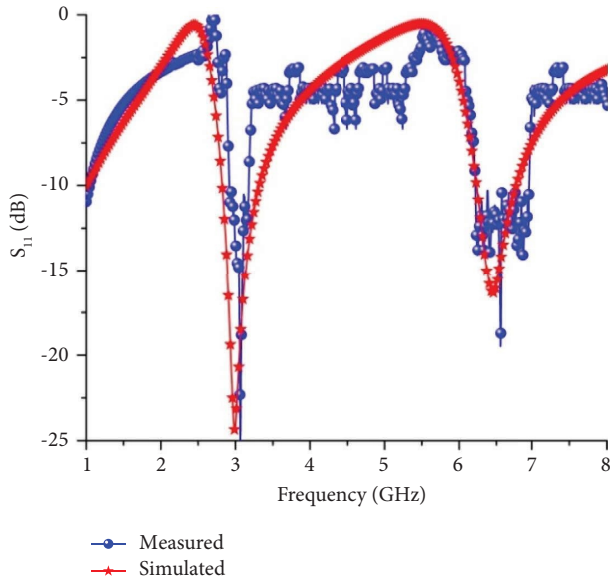

Figure 10: Measured and simulated S_{11} (dB) vs. frequency.

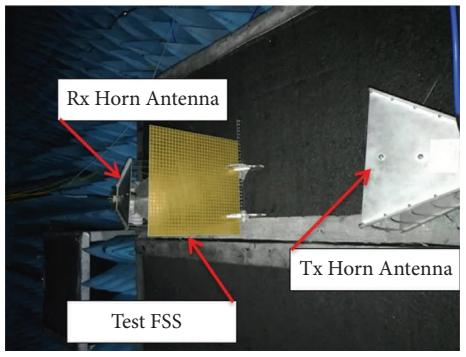

Figure 11: Scattering characteristic true measurement setup for proposed FSS.

Figures 12 and 13. However, the FSS has an acceptable agreement of calculated and measured outcomes.

The S_{21} execution of the double bandstop FSS is unaffected with polarized wavefronts; however, it has acceptable range of deviations in its S_{21} features up to 60° of incident angles. The measured and simulated TE and TM mode responses are presented in Table 1; it shows that the TE and TM modes have approximately equal bandwidths for Bluetooth and WLAN 0.3 GHz and 0.8 GHz, respectively. If the angle of incidence for TE and TM polarized wave is changed, the transmission and reflection characteristics of the convoluted meander line-inspired metallic surface filter will be affected. The change in the angle of incidence will affect the direction of the wave and the way it interacts with the filter, potentially changing the amount of energy that is transmitted and reflected. This could result in a shift in the frequency response of the filter, as well as changes in the insertion loss and return loss. The measured transmission coefficient of the FSS at different angles is presented in Table 2, which shows that the FSS has acceptable variations and also validated its polarization insensitivity. A comparative study of resonant frequency stability of proposed FSS and used references is presented in Table 3.

5. Performance Analysis of Proposed Design

The performance analysis of a convoluted meander line-inspired metallic surface filter (CMMSF) for Bluetooth and WLAN bands studies the filter's effectiveness in blocking Bluetooth and WLAN signals. This filter is designed to provide high rejection of signals in the Bluetooth and WLAN frequency bands while allowing signals outside these bands to pass through. The performance analysis looks at the filter's response to various Bluetooth and WLAN signals and its ability to reject them without affecting signals in other frequency bands. The performance analysis also looks at the filter's insertion loss (the amount of energy lost as a signal passes), return loss (the amount of energy reflected from the filter), and other parameters. The overall performance of the filter is measured and compared to other filters of the same type. It allows engineers to determine the best filter solution for their specific application.

5.1. Advantages

(i) Improved performance: the convoluted meander line-inspired metallic surface filter is designed to reduce interference from other radio frequencies and thus improve the performance of Bluetooth and WLAN bands.

(ii) Compact design: the filter is designed to be compact, making it easier to install and use with existing systems.

(iii) Low cost: the filter is made from metallic surfaces and does not require expensive components, making it cheaper than other filters.

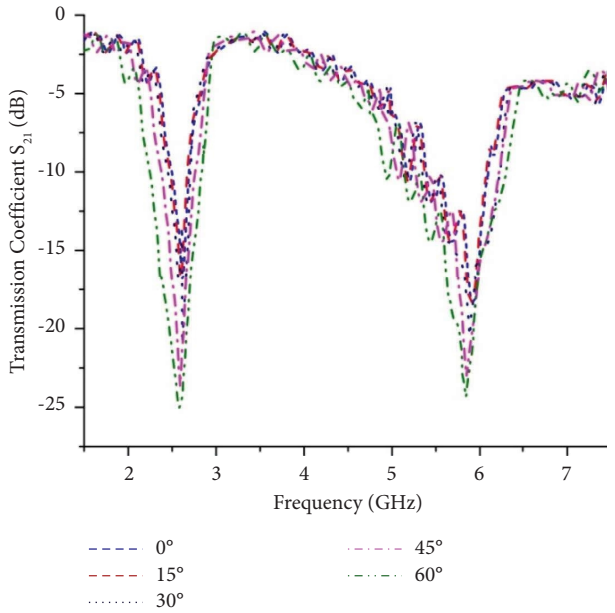

Figure 12: Measured transmission coefficient vs frequency for TE mode.

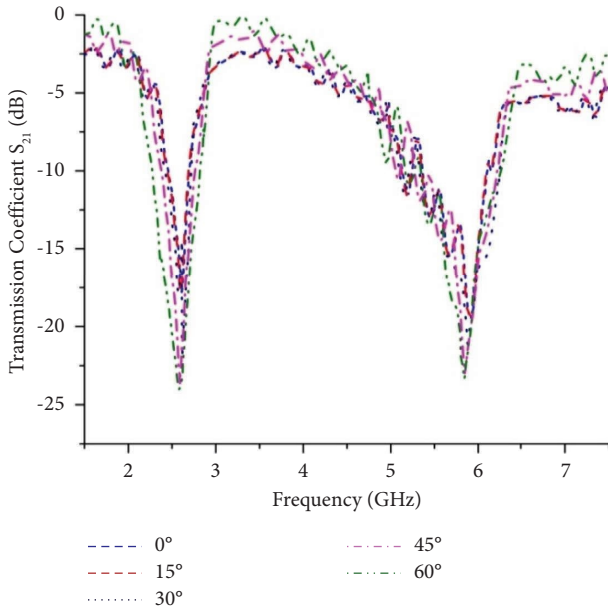

Figure 13: Measured transmission coefficient vs frequency for TM mode.

Table 1: Comparison of simulated and measured results.

Frequency bands	TE mode		TM mode	
	Simulated 10 dB BW	Measured 10 dB BW	Simulated 10 dB BW	Measured 10 dB BW
Band 1 (2.4 GHz)	2.3–2.6 GHz (0.3 GHz)	2.4–2.7 GHz (0.3 GHz)	2.33–2.58 GHz (0.25 GHz)	2.42–2.68 GHz (0.26 GHz)
Band 2 (5.5 GHz)	5.2–5.8 GHz (0.6 GHz)	5.3–6.1 GHz (0.8 GHz)	5.20–5.76 GHz (0.56 GHz)	5.37–6.09 GHz (0.72 GHz)

(iv) Low insertion loss: the filter has a low insertion loss, meaning it does not degrade the signal strength as it passes through.

(v) High isolation: the filter has high isolation, effectively blocking out interfering signals from other radio frequencies.

Table 2: Measured TE mode response of FSS at different incident angles.

Incident angle variation with bandwidth in TE mode					
Frequency bands	0 degree	15 degrees	30 degrees	45 degrees	60 degrees
Band 1 (2.4 GHz)	0.3 GHz	0.36 GHz	0.24 GHz	0.39 GHz	0.59 GHz
Band 2 (5.5 GHz)	0.8 GHz	0.87 GHz	0.72 GHz	0.95 GHz	0.96 GHz

Table 3: Proposed FSS characteristics in comparison to used references.

Reference	Size (mm^2)	Stop band (frequency)	Incident angle TE/TM	Frequency deviation
Bagci et al. [6]	30×30	2.4, 5.5 GHz	60° (TE/TM)	12%
Birwal et al. [22]	16×16	UWB	45° (TE/−)	11%
da Silva Segundo et al. [13]	18×19	2.4, 5.5 GHz	30° (TE/−)	9%
Döken and Kartal [9]	29.3×29.3	2.4, 5.8 GHz	60° (TE/TM)	5%
Hussein et al. [15]	22×22	2.36, 3.3 GHz	45° (TE/−)	3%
Kanchana et al. [17]	8×8	10, 12.1, 17.8 GHz	60° (TE/TM)	3%
Kocakaya and Çakır [7]	7.7×7.7	X-band	60° (TE/TM)	1%
Liu et al. [8]	6.2×6.2	3.2, 4.2, 5.4 GHz	60° (TE/TM)	0.9%
Present work	9.7×9.7	2.4, 5.5 GHz	60° (TE/TM)	3.2% at 2.4 GHz 2.9% at 5.5 GHz

5.2. Applications

(i) Use them to reduce interference in densely populated areas by blocking out unwanted signals.

(ii) Use them to improve the signal-to-noise ratio of Bluetooth and WLAN bands by reducing out-of-band noise.

(iii) Use them as an antenna-level filter to reduce the impact of multipath interference on Bluetooth and WLAN transmissions.

(iv) Use them to protect sensitive equipment (e.g., medical devices) from electromagnetic interference.

(v) Use them as a building-level filter to reduce the impact of external interference on Bluetooth and WLAN networks.

The size of the convoluted meander line-inspired metallic surface filter can limit its applications in compact systems. The size of the filter affects its performance, as larger filters can be more effective at blocking certain types of signals. Additionally, the filter requires some physical space to be installed, which could be a problem if space is limited in the system.

6. Conclusion

The investigated FSS design successfully produces dual-band reflection characteristics for Bluetooth and WLAN (2.4/5.5 GHz) bands. The designed FSS has miniaturization in its unit cell which also reflects that the overall size of the FSS array is a compact size ($0.0776\lambda \times 0.0776\lambda$) and a good candidate for shielding the low-profile systems from EMI due to the narrowband WLAN devices. The FSS has wide reflection bandwidth for Bluetooth and WLAN applications, so it can effectively diminish the possibility of electromagnetic interference due to the adjacent narrow band applications. The measured results of the prototype model of fabricated FSS are very close to the simulated model which validates the reliability of the proposed design. The effects and examination of suggested FSS indicated that it is the enhanced style of designing FSS for multiband performance.

6.1. Future Works. In order to improve the performance of the proposed model, there are the following works to be required as per the future work aspect:

(i) The filter is limited to the specific frequency bands of Bluetooth and WLAN and may not be effective in blocking other frequency bands.

(ii) The filter is limited in size and may not be suitable for applications requiring a large antenna.

(iii) The filter may be unable to effectively reduce signal reflections and multipath distortion.

Data Availability

The data used to support the findings of this study are available from the corresponding author upon request.

Conflicts of Interest

The authors declare that they have no conflicts of interest.

Acknowledgments

The authors are grateful to Prof. K. V. Srivastava, Indian Institute of Technology, Kanpur, India, for providing measuring facilities.

References

[1] B. A. Munk, *Frequency Selective Surfaces: Theory and Design*, John Wiley and Sons, New York, NY, USA, 2005.

[2] S. W. Schneider and B. A. Munk, "The scattering properties of "Super Dense" arrays of dipoles," *IEEE Transactions on Antennas and Propagation*, vol. 42, no. 4, pp. 463–472, 1994.

[3] S. Yadav, C. P. Jain, and M. M. Sharma, "Smartphone frequency shielding with penta-bandstop FSS for security and electromagnetic health applications," *IEEE Transactions on Electromagnetic Compatibility*, vol. 61, no. 3, pp. 887–892, 2019.

[4] R. J. Langley and E. A. Parker, "Equivalent circuit model for arrays of square loops," *Electronics Letters*, vol. 18, no. 7, pp. 294–296, 1982.

[5] I. Sohail, Y. Ranga, K. P. Esselle, L. Matekovits, and S. G. Hay, "Polarization stable ultra-wide-band frequency selective surface for ku- and K- band applications," in *Proceedings of the 2013 International Conference On Electromagnetics In Advanced Applications (ICEAA)*, pp. 802–805, Torino, Italy, September 2013.

[6] F. Bagci, C. Mulazimoglu, S. Can, E. Karakaya, A. E. Yilmaz, and B. Akaoglu, "A glass based dual band frequency selective surface for protecting systems against WLAN signals," *International Journal of Electronics and Communications*, vol. 82, pp. 426–434, 2017.

[7] A. Kocakaya and G. Çakır, "Novel angular-independent higher order band-stop frequency selective surface for X-band applications," *IET Microwaves, Antennas and Propagation*, vol. 12, no. 1, pp. 15–22, 2017.

[8] N. Liu, X. Sheng, C. Zhang, J. Fan, and D. Guo, "A miniaturized triband frequency selective surface based on convoluted design," *IEEE Antennas and Wireless Propagation Letters*, vol. 16, pp. 2384–2387, 2017.

[9] B. Döken and M. Kartal, "Easily optimizable dual-band frequency-selective surface design," *IEEE Antennas and Wireless Propagation Letters*, vol. 16, pp. 2979–2982, 2017.

[10] W. Li, S. Xia, H. Shi et al., "Design of a dual-band dual-polarization transparent frequency selective surface," *IEEE Antennas and Wireless Propagation Letters*, vol. 16, pp. 3172–3175, 2017.

[11] G. Xu, S. V. Hum, and G. V. Eleftheriades, "A technique for designing multilayer multistopband frequency selective surfaces," *IEEE Transactions on Antennas and Propagation*, vol. 66, no. 2, pp. 780–789, 2018.

[12] W. Yin, H. Zhang, T. Zhong, and X. Min, "A novel compact dual-band frequency selective surface for GSM shielding by utilizing a 2.5-dimensional structure," *IEEE Transactions on Electromagnetic Compatibility*, vol. 60, no. 6, pp. 2057–2060, 2018.

[13] F. C. G. da Silva Segundo and A. L. P. S. Campos, "Compact frequency selective surface with dual band response for WLAN applications," *Microwave and Optical Technology Letters*, vol. 57, no. 2, pp. 265–268, 2015.

[14] T. Zhong, H. Zhang, R. Wu, and X. Min, "Novel dual-band miniaturized frequency selective surface based on fractal structures," *Frequenz*, vol. 71, no. 1-2, pp. 57–63, 2017.

[15] M. Hussein, J. Zhou, Y. Huang, M. Kod, and A. P. Sohrab, "Dual stopband frequency selective surface by using half rings and slots," *Microwave and Optical Technology Letters*, vol. 58, no. 5, pp. 1136–1139, 2016.

[16] W. Li, C. Wang, Y. Zhang, and Y. Li, "A miniaturized frequency selective surface based on square loop aperture element," *International Journal of Antennas and Propagation*, vol. 2014, Article ID 701279, 6 pages, 2014.

[17] D. Kanchana, S. Radha, B. S. Sreeja, and E. Manikandan, "Polarization dependent FSS for X and Ku-band frequency response," *Journal of Optoelectronics and Advanced Materials*, vol. 22, pp. 365–370, 2020.

[18] M. Bahadorzadeh and C. F. Bunting, "A dual band-reject FSS for WI-FI application," in *Proceedings of the 2018 International Applied Computational Electromagnetics Society Symposium (ACES)*, pp. 1-2, Centennial, CO, USA, March 2018.

[19] Y. Yang, W. Li, K. N. Salama, and A. Shamim, "Polarization insensitive and transparent frequency selective surface for dual band GSM shielding," *IEEE Transactions on Antennas and Propagation*, vol. 69, no. 5, pp. 2779–2789, 2021.

[20] M. M. Zargar, A. Rajput, K. Saurav, and S. K. Koul, "Polarisation-insensitive dual-band transmissive rasorber designed on a single layer substrate," *IET Microwaves, Antennas and Propagation*, vol. 14, no. 11, pp. 1296–1303, 2020.

[21] J. Dong, Y. Ma, Z. Li, and J. Mo, "A miniaturized quad-stopband frequency selective surface with convoluted and interdigitated stripe based on equivalent circuit model analysis," *Micromachines*, vol. 12, no. 9, p. 1027, 2021.

[22] A. Birwal, S. Singh, and B. K. Kanaujia, "A novel design of ultra-wide stop-band single-layer frequency selective surface using square-loop and cross," *International Journal of Microwave and Wireless Technologies*, vol. 13, no. 8, pp. 800–809, 2021.

[23] K. Katoch, N. Jaglan, S. D. Gupta, and M. S. Sharawi, "Design of a triple band notched polarization independent compact FSS at UWB frequency range," *International Journal of RF and Microwave Computer-Aided Engineering*, vol. 31, no. 6, Article ID e22631, 2021.

[24] K. Katoch, N. Jaglan, and S. D. Gupta, "Design and analysis of single sided modified square loop UWB frequency selective surface," *IEEE Transactions on Electromagnetic Compatibility*, vol. 63, no. 5, pp. 1423–1432, 2021.

[25] K. Katoch, N. Jaglan, and S. D. Gupta, "Analysis and design of a simple and compact bandstop Frequency Selective Surface at mobile WiMAX and satellite communication X-band," *Journal of Electromagnetic Waves and Applications*, vol. 35, no. 10, pp. 1321–1336, 2021.